MEGA JOURNAL OF CASE REPORTS

OPEN ACCESS

Review Article

Compiled Date: June 06, 2025

Thermal Product Sensing: Simulations and Experiments of a Novel Biosensor for Quantitative Thermal Property Measurement of Biological Tissues

Nathalie Nick[1]*, Joe Kirkup[1], Marcus Allen[1], Parv Sains[2] and Kam Chana[1]

[1]Department of Engineering Science University of Oxford, United Kingdom

[2]SainsSurgical. 4 Elsworthy, Thames Ditton, Surrey, KT7 0YP, UK

[*]**Corresponding author**: Nathalie Nick, Department of Engineering Science University of Oxford, Osney Mead, Oxford, OX2 0ES, United Kingdom

Abstract

Skin cancer represents a critical global health challenge, with incidence rates rising dramatically over recent decades. In the UK, the incidence of malignant melanoma has increased from 837 per year to 6963 per year in males and 1609 per year to 6952 per year in females between 1981 and 2018. Current diagnostic methods rely on time-consuming biopsy and histopathological analysis, which can delay critical intervention. This study uses a Thermal Product Sensor (TPS), a technology proven in aerospace engineering applications, now transferred to biomedical applications. This new and innovative biosensor is designed to provide rapid, quantitative assessment of biological tissue thermal properties. The Thermal Product sensor employs a measurement technique utilizing platinum thin-film gauges on a Macor substrate to directly measure thermal transfer characteristics. Through detailed mathematical modeling and experimental validation, the sensor's capability to distinguish between different biological tissue types with high precision is demonstrated. The sensor's working principle is grounded in fundamental heat transfer principles, specifically leveraging the relationship between thermal conductivity, density, and specific heat capacity.

Experimental validation using porcine tissue samples revealed the sensor's ability to differentiate between skin, fat, and muscle tissues with 99.9% confidence. Furthermore, the study investigated the impact of

medical films on thermal measurements, showing minimal interference for skin tissues and providing crucial insights for potential clinical applications. A numerical heat transfer model was developed - utilising both the one-dimensional heat diffusion equation and Pennes' bioheat equation - to increase understanding of the detrimental effect on sensitivity of a plastic medical film and to aid in future design optimisation. Thermal responses to cancerous and non-cancerous tissue were investigated, exploring the sensors potential as a diagnostic tool.

Keywords: Thermal biosensor; Skin cancer detection; Heat transfer measurement; Thermal product sensor; Biological tissue characterization; Non-invasive diagnostics; Thermal properties

Introduction

Skin cancer is currently an escalating global public health problem. In the United Kingdom, within 37 years between 1981 and 2018 the incidence of malignant melanoma has increased from 837 to 6963 per year in males and 1609 to 6952 per year in females. Early diagnosis and treatment, as with any disease, has a positive outcome on survival and costs of management. However, with the current gold standard in skin cancer detection – biopsy followed by histopathological analysis – it takes weeks if not even months for the results, a time span within which the cancer is spreading. Hence, a rapid – in the best case real-time – diagnosis tool is highly favourable. Advances in technology have allowed the development of tools that provide rapid and sensitive diagnosis of many diseases. The development and use of a new biosensor, the Thermal Product Sensor (TPS), is described in this paper. Skin is the largest organ of the human body. It has many functions including protection of deeper biological layers, heat regulation, secretion, sensation, and absorption. The structure of skin comprises two layers, the epidermis and dermis. The outermost layer, the epidermis, is composed of keratinocytes, Merkel cells, and Langerhans's cells. It is in this layer that most skin cancers arise **[1].** According to Zhang et al **[2]**, in 2019 there were 4.0 million Basal Cell Carcinomas (BCC), 2.4 million Squamous Cell Carcinomas (SCC), 0.3 million Malignant skin Melanomas (MSM). As a result, there were approximately 62'800 deaths and 1.7 million Disability-Adjusted Life Years (DALYs) due to MM, 56'100 deaths and 1.2 million DALYs secondary to SCC, respectively. This highlights the economic and healthcare burden caused by skin cancer. The diagnosis of skin cancers, relies upon clinical review and visual inspection, usually followed by dermoscopic examination and biopsy with histological analysis. Other technologies have also been developed to improve the diagnoses of skin cancers **[3]**. The purpose of new technologies is to provide rapid, non-invasive, highly sensitive and possible remote diagnosis of skin cancers. However, new technologies are limited by high expenses, low specificity, and the requirement of specially trained, qualified operators. Biosensors are technological devices with the ability to sense the difference between various biomolecules. They are integrated receptor-transducer devices that convert biological responses to electrical signals. The use of biosensors in healthcare with a diversity of applications has been widely reported. The application of thermal product in the diagnosis of skin cancers is a new method achieved using the TPS. Thermal product dictates the amount of heat absorbed by the material it comes into contact with. The measurement is dependent on density (ρ), specific heat capacity (c) and thermal conductivity (κ) of the material. This energy transfer

is quantified by directly measuring temperature which can be recorded. The aim of this study is to explore the application of skin cancer diagnosis with the TPS and facilitate the testing of the TPS in clinical trials. A sensor was calibrated and tested on real porcine skin as a proof of concept. The feasibility of distinguishing between normal skin, benign skin lesions, and malignant lesions was later tested using simple logistic regression and SVMs trained on data of 12 patients reported by Nick et al. **[4].**

Sensor Details

The proposed solution to the early-stage skin cancer diagnosis problem lies in a hand-held biosensor **(Figure 1)** pioneered by Professor Kam Chana and PrOxisense LTD in the Oxford University Thermo-Fluids laboratory in Oxford, UK. The sensor body is a 10cm long cylinder of 1cm diameter. At the measuring end is the substrate bottom made up of Macor (a vitreous glass). Two thin filaments of platinum, a few microns thick, are hand-painted onto the substrate to be ≈8 mm long, <1mm wide, and are connected to the sensor body through gold contacts.

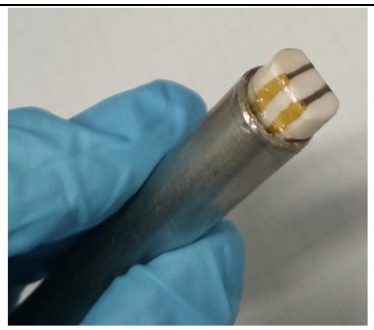

Figure 1: Platinum and Gold TP biosensor.

Sensor Working Principle

The sensor's fundamental working principle is based on measuring the Thermal Product (TP) of the material that is in contact with the sensor by applying a pulse of heat. A platinum thin-film gauge is painted on an insulating disc made of Macor substrate, which makes up the contact surface of the sensor bottom. When an electrical square pulse of known amplitude and duration is passed through the sensor, the sensor heats up from electrical resistance. This heat is dissipated between the sensor substrate bottom and the material in contact with the sensor, and the increase in temperature of the sensor is measured by the thin-film gauge **(Figure 2)**. Changes in the surrounding material composition will affect the split in dissipated heat between the sensor substrate bottom and the surrounding material, an effect which correlates with the TP of the surrounding material.

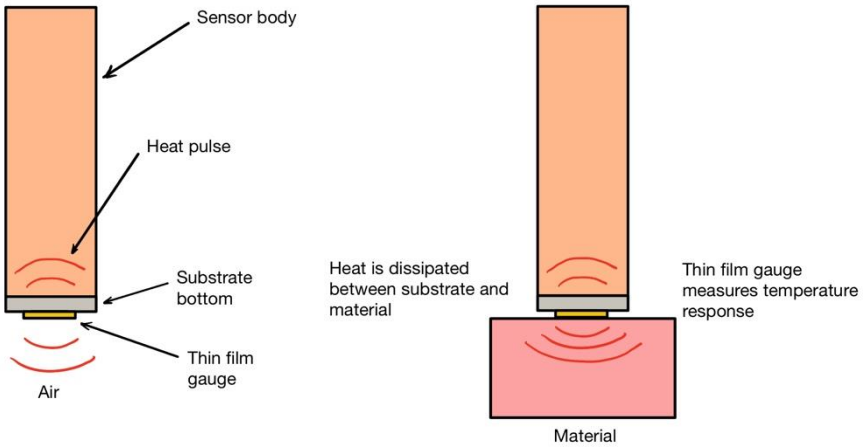

Figure 2: Probe delivers heat pulse wave and measures temperature rise with thin-film gauge. The heat dissipated changes based on properties of surrounding material.

Sensor Mathematical Background

The theory behind the sensor can be modelled by drawing a boundary around the material to be measured, with a constant heat input $_{qm(t)}$ applied by the sensor **(Figure 3)**.

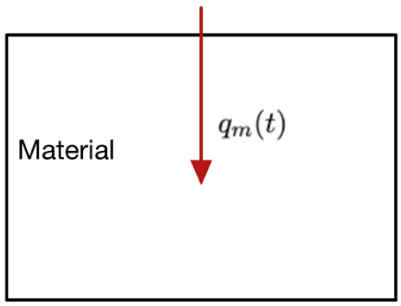

Figure 3: Simplified model of sensor.

Using this simplified model, the material is in equilibrium with its surroundings and there is no internal heat generation. 1-dimensional isotropic conduction, the Fourier law of heat conduction shows the relationship between heat transfer and temperature change:

$$q(t) = -k\frac{\partial T}{\partial x}$$

Where q(t) is the heat flux, the temperature is T at distance x from the contact surface at time t, and k is the thermal conductivity. Taking an infinitesimally small volume of material, the energy balance in the x direction in a small interval of time δt can be written as:

$$Q(x) - Q(x + \partial x) = \rho A\, \partial x c \frac{\partial T}{\partial t}$$

$$\frac{\partial}{\partial x}\left(-kA\frac{\partial T}{\partial x}\right)\partial x = \rho A\, \partial x c \frac{\partial T}{\partial t}$$

This gives the sensor's temperature response in the form of the 1-dimensional transient heat conduction equation:

$$\frac{\partial^2 T(x,t)}{\partial x^2} = \frac{1}{\alpha(x)} \frac{\partial T(x,t)}{\partial t}$$

Where α is the heat diffusivity of the material, ρ is density and c is the specific heat capacity.

$$\alpha = \frac{k}{\rho c}$$

Analytical Solution

A step voltage pulse of known amplitude from a constant current for a fixed duration is applied by the sensor to generate heat, which will produce a thermal response curve in the platinum thin-film gauge, as shown in **Figure 4**.

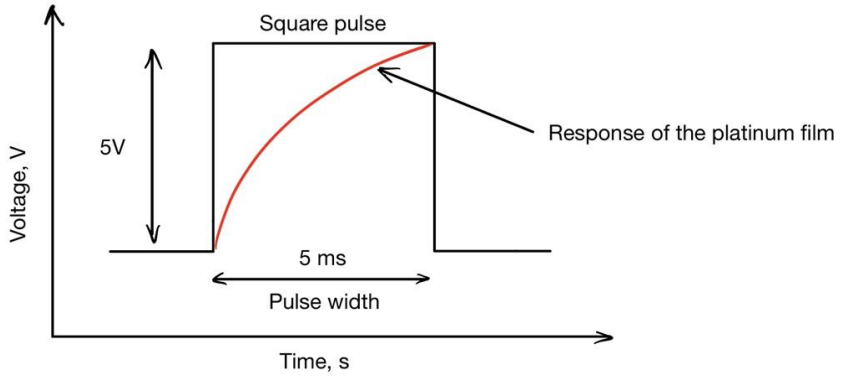

Figure 4: Square wave applied by the sensor and thin-film response.

An analytical solution can be derived for the response to a square pulse, with the following boundary and initial conditions derived from the assumptions stated previously:

- The first boundary condition comes from a semi-infinite assumption such that the temperature of the material and substrate will be unchanged from the ambient temperature at an infinite distance away from the platinum filament.

$$\Delta T(x \to \infty, t) = 0$$

- The second boundary condition states that the contact point (x = 0) between the measured material and the platinum filament is defined by the Fourier law of heat conduction.

$$\frac{\partial T}{\partial x}\Big|_{x=0} = \frac{-q_m(t)}{k}$$

- The initial condition assumes the material and substrate are in equilibrium with the surroundings, such that they start at ambient temperature at time t = 0.

$$\Delta T(x, t = 0) = 0$$

The analytical solution can be derived by taking the Laplace transform of the 1-dimensional transient heat conduction equation. Using the initial conditions, we obtain:

$$\frac{\partial^2 \bar{T}}{\partial x^2} = \frac{s}{\alpha} \bar{T}$$

where T̄(x, s) denotes the Laplace transform of T . This gives a general solution in the form:

$$\bar{T} = Ae^{\sqrt{\frac{s}{\alpha}}x} + Be^{-\sqrt{\frac{s}{\alpha}}x}$$

Transforming the boundary conditions into Laplace space allows us to substitute them into the general solution and find coefficients A and B. The first boundary condition gives A = 0, and the second boundary condition gives:

$$B = \frac{\bar{q}_m}{k}\sqrt{\frac{\alpha}{s}}$$

and thus, the overall temperature response is:

$$\bar{T} = \frac{\bar{q}_m}{k}\sqrt{\frac{\alpha}{s}}e^{-\sqrt{\frac{s}{\alpha}}x}$$

To find a specific solution, the heat input function $\bar{q}_{m(s)}$ must also be defined. As discussed, the input function in the time space, $q_m(t)$, is a square pulse, but for the thermal response, only the initial unit step from time t = 0 with an amplitude of q_m is considered, which has the standard Laplace transform:

$$\mathcal{L}[\bar{q}_m(t) = u(t)] = \bar{q}_m = \frac{q_m}{s}$$

Substituting q_m/s into the temperature response equation in the Laplace space gives:

$$\bar{T} = \frac{q_m}{k}\sqrt{\frac{\alpha}{s^3}}e^{-\sqrt{\frac{s}{\alpha}}x}$$

To convert this equation back into time space, an existing standard inverse of this Laplace equation is used to produce the solution:

$$\Delta T(x,t) = \frac{q_m\sqrt{\alpha}}{k}\left[\frac{2\sqrt{t}}{\sqrt{\pi}}e^{-\frac{x^2}{4\alpha t}} - \frac{x}{\sqrt{\alpha}}\text{erfc}\left(\frac{1}{2}\sqrt{\frac{x^2}{4\alpha t}}\right)\right]$$

Finally, taking a temporal solution at the point of contact between the filament and the material (i.e. x = 0), and expanding out α, the solution reduces to:

$$\Delta T(x=0,t) = \frac{q_m}{\sqrt{\rho ck}}\frac{2\sqrt{t}}{\sqrt{\pi}}$$

where $\sqrt{\rho ck}$ is the thermal product of the measured material. The solution in this form clearly shows an inverse square root relationship between temperature T and the TP.

Penetration Depth

A longer pulse length will allow greater penetration into the material, which allows detection of biological features of greater depth. To derive the relationship between pulse length and penetration depth, the heat penetration depth x_{pen} will be taken as the distance at which the heat flux q_m or the temperature T is at 1% of its original value at the surface, i.e.:

$$\frac{q_m(x = x_{pen}, t)}{q_m(x = 0, t)} = 0.01$$

$$\frac{\Delta T(x = x_{pen}, t)}{\Delta T(x = 0, t)} = 0.01$$

Now taking the thermal response equation for ΔT(x,t) at depth x, the Fourier law can be used to express the heat transfer variation with depth x:

$$q_m(x,t) = -k\frac{\partial T}{\partial x} = q_m(x=0,t)\,\text{erfc}\left(\frac{1}{2}\sqrt{\frac{x^2}{4\alpha t}}\right)$$

Introducing a dimensionless penetration depth $x^* = x/\sqrt{4\alpha t}$, the ratios of heat flux and temperature with that at the surface reduce to:

$$\frac{q_m(x^*,t)}{q_m(x=0,t)} = \text{erfc}(x^*)$$

$$\frac{\Delta T(x^*,t)}{\Delta T(x=0,t)} = e^{-x^{*2}} - \sqrt{\pi}x^*\text{erfc}(x^*)$$

These ratios describe the normalized heat flux and temperature variation with depth in the material, as plotted in **Figure 5**. For a 1% heat flux penetration and temperature penetration, the dimensionless depth was found to be $x^* = 1.82$ and $x^* = 1.58$ respectively.

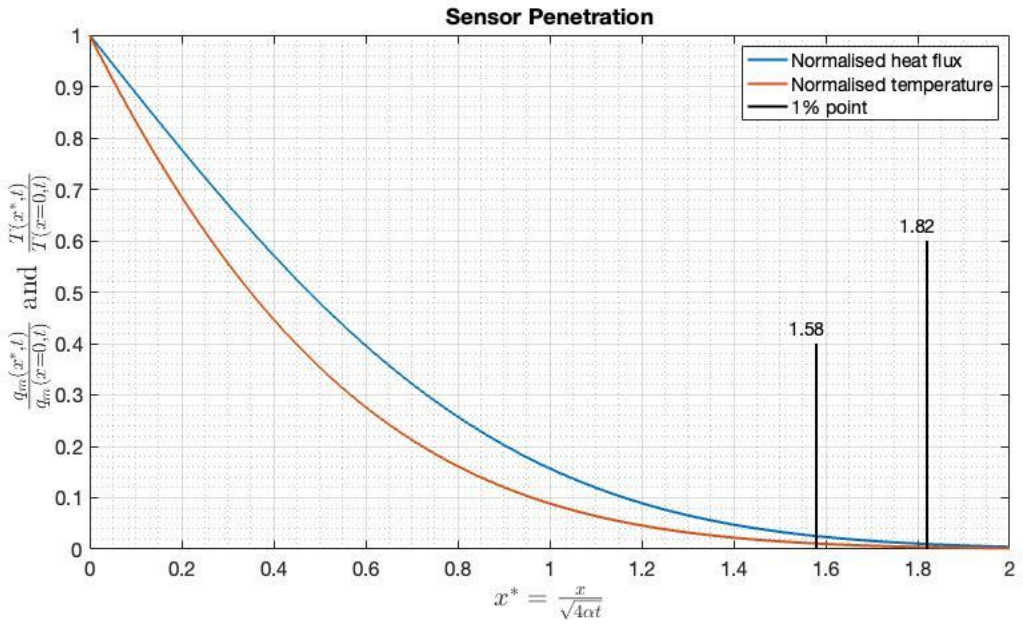

Figure 5: Normalized heat flux and temperature variation with depth.

Converting dimensionless penetration depth x^* back into absolute penetration depth x_{pen}, it is found that x_{pen}= 3.64 √αt and x_{pen}= 3.16 √αt for heat flux and temperature to be 1% of their surface values, respectively. The two criteria for penetration depth are so close that a rule of thumb can be conveniently written as:

$$x_{pen}(cm) \approx 4\sqrt{\alpha t}$$

In practice, for a conservative estimate that considers the limited sensitivity and precision of a given sensor, the penetration depth is often quoted [5] as:

$$x_{pen}(cm) \approx \sqrt{\alpha t}$$

where x^*= 0.5. At this depth, the normalized heat flux $^{q_m(x^*,t)}/_{q_m}$ (x=0,t) = 0.480, and the normalized temperature $^{\Delta T(x^*,t)}/_{\Delta T}$ (x=0,t) = 0.354, such that a change in TP would produce a significant effect on the output signal.

Method

The biological tissue selected for testing was porcine due to its similarities in thermal and mechanical properties with human skin [6]. "A large pork belly sample with multiple layers of tissue (Figure 9) such as skin, fat, muscle fascia and muscle has been tested".

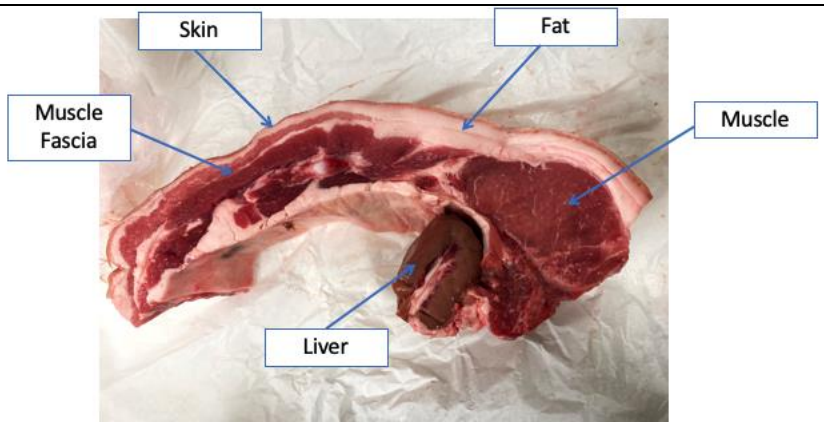

Figure 9: Different tissue layers in pork belly.

The sensor was pressed into the tissue and held via a clamp to ensure the platinum contact surface area remained constant, as small movements would drastically change the measurements. The process is shown in **Figure 10** below.

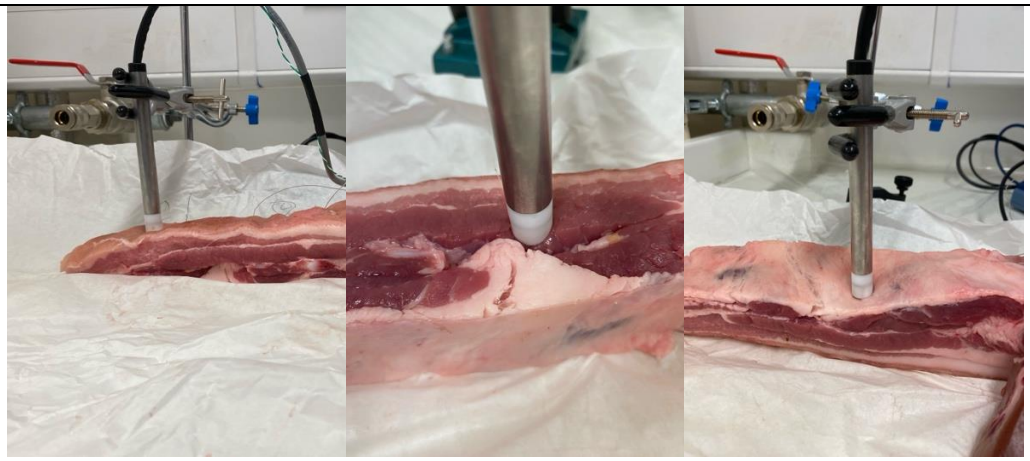

(a) Skin measurement. (b) Muscle measurement. (c) Fat measurement.

Figure 10: Thermal response measurement of three types of tissue.

To retrieve thermal response graphs and extract the TP, the following steps were taken:

- Convert Voltage ($\bar{V}$) response to Temperature (T) using the sensor's calibrated Seeback coefficient $\sigma = 0.0053$ [V/C].
- Convert sample number (i) to time (t) using the sample rate.
- Remove the first 15 sample points of each pulse before the measurements stabilize.
- Shift data in temperature (T) and time (t) to start at $\Delta T = 0$, $t = 0$.
- Extract TP using the numerical interpolation of the relationship between TP and ΔT.

Porcine Experimentation

To validate the sensor's potential for medical applications, a proof-of-concept study using porcine tissue as a biologically relevant model has been conducted. Given the ethical and practical constraints of obtaining live cancerous skin samples, porcine tissue provided an ideal experimental substrate due to its thermal and mechanical similarities to human tissue. The initial experiment focused on characterizing the thermal response across different biological tissue types. Specifically, skin, fat, and muscle regions from a pork belly sample were examined, taking precise measurements from three distinct locations within each tissue type. The resulting thermal response curves, presented in **Figure 6**, reveal distinctive thermal signatures that demonstrate the sensor's capability to differentiate between tissue types with remarkable precision.

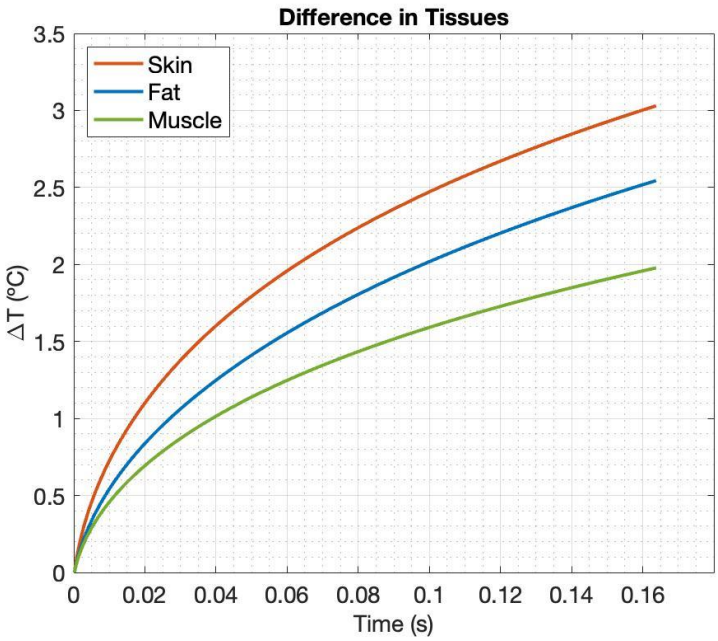

Figure 6: Thermal responses of different porcine tissues.

The graph clearly shows significantly different measured thermal responses for skin, fat and muscle. Their respective extracted thermal products are TP_{skin}= 1195, TP_{fat}= 1380 and TP_{muscle}= 1552. The standard deviation of ΔT data from each series of 10 pulses was approximately 0.15ºC. This means the sensor should be able to distinguish between these three tissues with ≈99.9% confidence under this setup. The measured thermal response curves and extracted TP values for skin, fat and muscle are consistent with previous experiments done with the sensor **[7].** Muscle is generally shown in the literature to have the highest thermal conductivity of the three, while fat and skin have lower conductivities **[8].** This thermal characteristic aligns with the biological function of these tissues, where fat and skin serve as protective thermal barriers, minimizing heat loss and maintaining core body temperature. The experiment demonstrates the sensor's capability to distinguish between biological tissues with different Thermal Products (TPs) with high accuracy. While valuable for surgical applications, the critical potential lies in

extending this approach to differentiate between cancerous and non-cancerous lesions in vivo, contingent upon measurable TP variations.

Effect of Medical Film

The second experiment investigated the impact of medical film on thermal responses across porcine tissue types. For skin, **Figure 7** reveals thermal response curves that are nearly identical, with the medical film causing a marginally lower ΔT. The extracted thermal product with the film (TP_{skin-f} = 1215) differed from the bare skin measurement (TP_{skin} = 1195) by only 1.7%, demonstrating minimal interference in thermal property measurements.

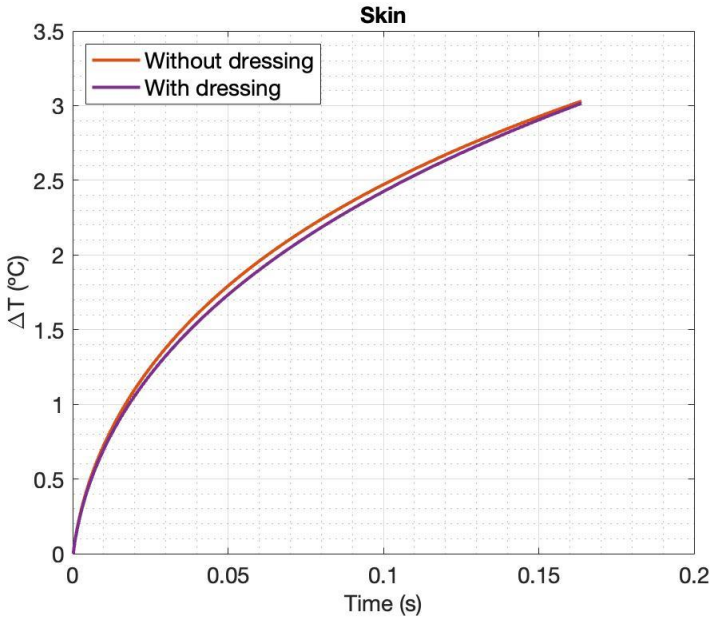

Figure 7: Thermal responses of porcine skin with and without medical dressing.

The film's minimal impact on skin measurements can be explained by its negligible thickness (x_{film} = 47μm), which corresponds to a pulse duration of 0.3ms. This brief interaction ensures that the skin's thermal product quickly dominates the measurement, ensuring the film does not interfere with diagnostic measurements. In contrast, **Figure 8** reveals that the medical dressing significantly alters thermal responses for fat and muscle tissues, introducing substantial variations in their thermal product measurements.

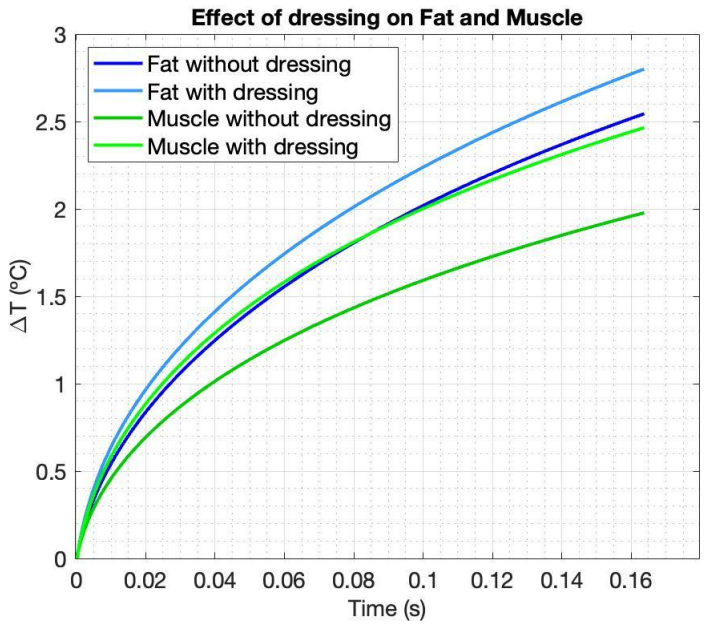

Figure 8: Thermal responses of fat and muscle, with and without medical dressing.

The extracted thermal products were TP_{fat} = 1380 and TP_{muscle} = 1552, compared to the dressed values of TP_{fat-f} = 1291 and $TP_{muscle-f}$ = 1385, which equates to large negative deviation errors of 6.4% and 10.7% respectively. This suggests the film causes a decrease in the measured thermal product, which is likely a product of one or a combination of three causes:

- The uneven surface of muscle and fat tissue caused air gaps to exist. The introduction of a medical film caused a layer of water to stick to the bottom of the film and fill the air gaps.
- The introduction of the medical film electrically insulated the porcine from the sensor, thus greatly reducing the effects of shorting. This allowed for a more accurate measurement of TP.
- The soft surfaces of muscle and fat tissue caused the medical film to crease despite attempts to minimize this. This created inconsistent thicknesses of film and may also have left air gaps between the sensor and the film, resulting in a lower TP.

Numerical Heat Transfer: Modelling Setup

To aid in future design optimisation and understand the losses incurred by the introduction of the plastic covering a numerical heat transfer model was created. The approach adopted to solve the model was the 'method of lines (MOL)': discretising the spatial derivative and using a variable-order implicit multistep method to solve the resulting Ordinary Differential Equation (ODE) in time. This was achieved using the PDEPE function in MATLAB 2022a.

The governing equation of the plastic film is the 1D heat diffusion equation expressed in Cartesian coordinates with no internal heat generation as detailed in Sensor Mathematical Background. As the domain transitions to human tissue the governing equation changes to the Pennes' bioheat equation:

$$\frac{1}{\alpha(x)_i}\frac{\partial T(x,t)}{\partial t} = \frac{\partial^2 T(x,t)}{\partial x^2} - \lambda_i(T(x,t) - T_c) + \frac{q_{met,i}}{k_i}$$

The tissue decay constant is $\lambda_i = \frac{\omega_{b,i}\rho_i c_i}{k_i}$, where $\omega_{b,i}$ is the blood perfusion rate, $q_{met,i}$ is the metabolic heat production and T_c is the core body temperature; all in the domain material i. An abstracted diagram of the continuous spatial domain can be seen in **Figure 9**.

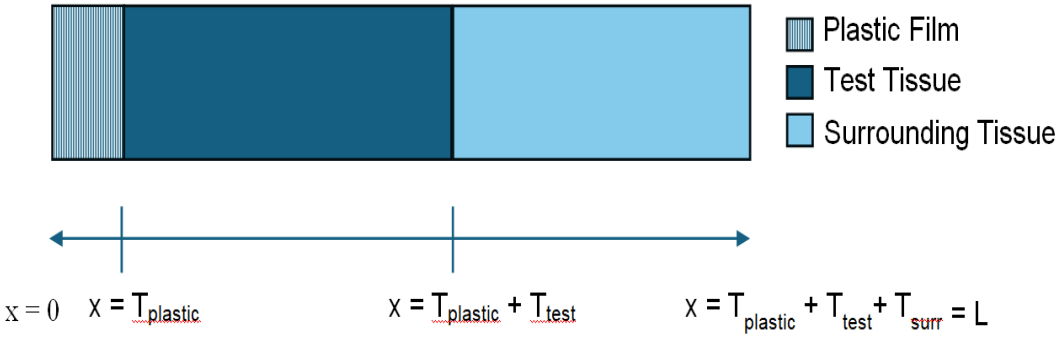

Figure 9: Abstracted representation of the multi-layered continuous 1D domain of the model.

The spatiotemporal domains were discretised to enable numerical analysis in finite steps. The spatial domain is represented by $x \in [0, L]$ divided into N intervals, $x_i = i\Delta x$, where $i = 0,1,2\ldots N$ and

$$\Delta x = \frac{L}{N}.$$

The quantity L is the total spatial domain length. The temporal domain is represented by $t \in [0, t_{end}]$ divided into M intervals, $t_i = i\Delta t$, where $i = 0,1,2\ldots M$ and $\Delta t = \frac{t_{end}}{M}$. The quantity t_{end} is the simulation end time.

Initial conditions of the system are required for the entire spatial domain. Body temperature as a function of the skin surface temperature T_{surf} (and other parameters previously defined) can be expressed as:

$$T(x,0) = T_c + (T_{surf} - T_c)e^{-\lambda_i x}$$

Boundary conditions are required, and are expressed as piecewise Neumann type conditions:

$$-k_i\frac{\partial T(L,t)}{\partial x} = 0$$

$$-k_i\frac{\partial T(0,t)}{\partial x} = \begin{cases}(1-\beta)q_0, & 0 < t \le t_{pulse}\\ 0, & t > t_{pulse}\end{cases}$$

t_{pulse} is the time length of the thermal step change pulse and $q_0 = \frac{I^2}{R}\frac{1}{A}$ where I is the electronic pulse current, R is the thin film resistance, and A is the cross-sectional area of the thin film. A 'heat split factor' was defined as:

$$\beta = \frac{\sqrt{\rho_{surf}c_{surf}k_{surf}}}{\left(\sqrt{\rho_{surf}c_{surf}k_{surf}} + \sqrt{\rho_{macor}c_{macor}k_{macor}}\right)}$$

to account for the fraction of the heat energy entering the Macor substrate (i.e. not directed into the tissue sample).

Numerical Heat Transfer: Spatial Mesh Convergence Study

Finite difference points chosen must have a small enough Δx to accurately capture the thermal behaviour in a reasonable computation time and ensure mesh size independence. Therefore, a mesh convergence study was performed where a set of N intervals was defined based on the equation $N = (1.2 \times 10^5) \times 2^{-k}$, where k ranges from 0 to 7, and the 1.2×10^5 constant was chosen based on computational resource restrictions. Solutions were computed for all resulting Δx, and the l^2 error norm calculated for all timepoints where $k = 0$ is considered the reference solution. This is shown in **Figure 10** below.

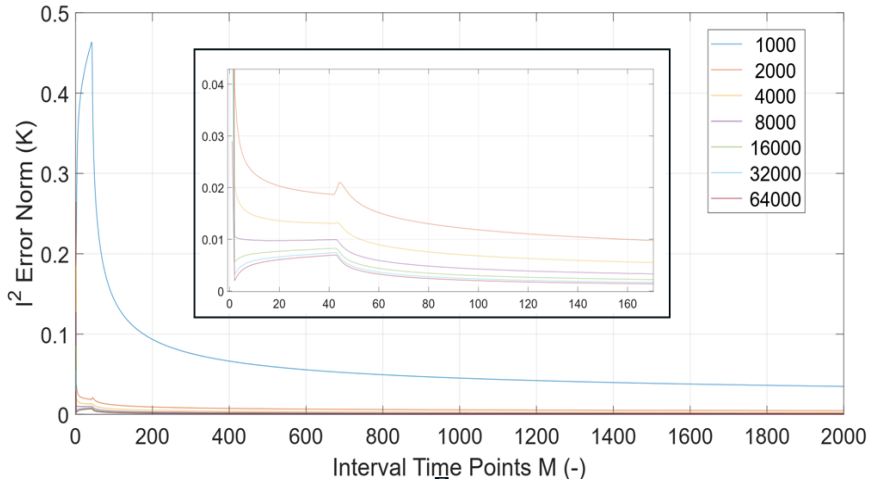

Figure 10: Plot of the l^2 error norm vs. interval point within the temporal domain.

A clear decrease in error norm can be seen approximately in-line with the expected convergence order; however, the discontinuities introduced by transition from the general 1D heat equation to Pennes' bioheat equation are evident. This may cause deviation from the expected convergence order value and raise the average l^2 error norm across the domain. Average error norms in the region of 10^{-4} were calculated for $k = 1$, which aligns with our convergence criteria. Consequently, this mesh density was utilised for all subsequent computational results. Absolute error and relative error tolerances were set at 10^{-8} and 10^{-6}, respectively.

Numerical Heat Transfer: Baseline Results

A baseline simulation was performed using the settings detailed in **Table 1**, and the probe geometry outlined in previous sections. All simulations set an initial skin surface temperature of 307.15K and a core body temperature of 310.15K.

Table 1: Baseline study details including all simulation parameter values not already disclosed **[9-11].**

Parameter Name	Value	Unit
Plastic Thickness	50	μm
Test Skin Thickness	10	mm
Surrounding Skin Thickness	10	mm
Pulse Current	800	mA
Thin Film Resistance	1.6	Ω
Cancerous Skin Thermal Properties		
Thermal Conductivity	0.25	W / m K
Specific Heat Capacity	3750	J / kg K
Mass Density	1030	kg / m^3
Metabolic Rate	3074	W / m^3
Blood Perfusion Rate	$2.6x10^{-3}$	ml / ml s
Normal Skin Thermal Properties		
Thermal Conductivity	0.187	W / m K
Specific Heat Capacity	3400	J / kg K
Mass Density	1060	kg / m^3
Metabolic Rate	368.1	W / m^3
Blood Perfusion Rate	$8.5x10^{-4}$	ml / ml s
Plastic Film Thermal Properties		
Thermal Conductivity	1.46	W / m K
Specific Heat Capacity	790	J / kg K
Mass Density	1704	kg / m^3

Figure 11 below displays the domain temperature as a function of the x-coordinate (or distance into the domain) and time. Down sampling of the solution was performed to retain gridlines whilst keeping the plot legible. Limits were also imposed on the x-axis and y-axis as it was discovered that the surrounding skin portion was irrelevant due to the minimal penetration depth.

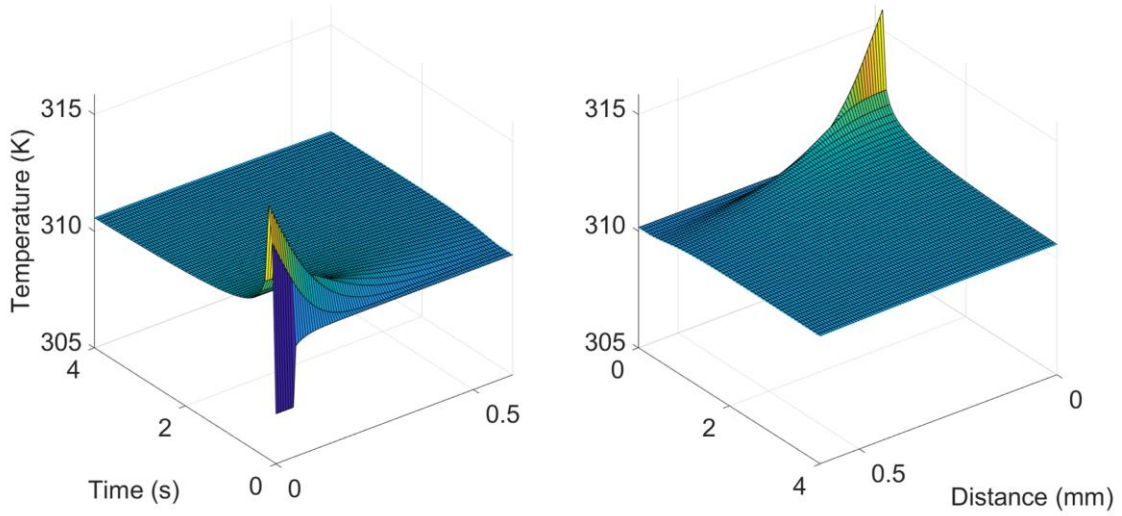

Figure 11: Surface plots of the domain temperature against x-coordinate and time. Both left and right plots are identical aside from being rotated for ease of understanding.

The initial condition of an exponential temperature rise with increasing skin depth can be seen clearly on the left surface plot, with the plastic temperature and skin surface temperature being 307.15K and rising to a core body temperature of ~310.15K within a depth of 275μm from the surface. As a result of the thermal pulse heating, the domain temperature sharply rises to its peak of 315.9K at the skin surface within ~0.16 seconds. This larger surface temperature causes thermal energy to diffuse into the skin; however, the penetration is limited by both the poor thermal diffusivity of tissue material and blood perfusion removing energy from the test skin location. The skin surface takes approximately 10 seconds to return to core body temperature. This is a substantial overestimate, as the platinum thin film and Macor substrate will not act as an adiabatic boundary and will in-fact enable back diffusion of thermal energy from the skin surface to the probe.

Figure 12 below displays the temperature as a function of time where each legend entry is a point of interest (POI) within the spatial domain. The temporal domain has been limited to 0.35 seconds, enlarging the region of the early thermal pulse response.

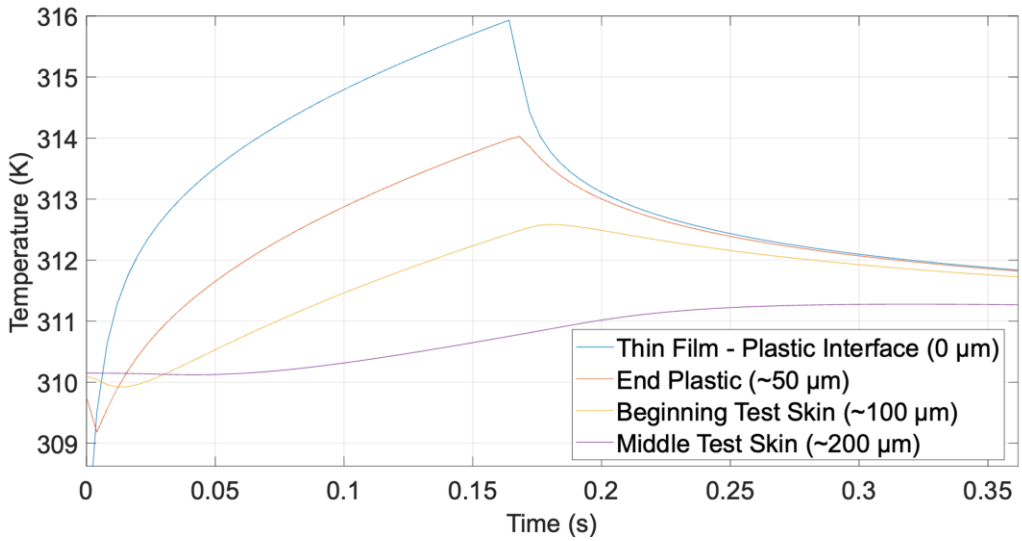

Figure 12: Line plot of the domain temperature against time at various POI such as material interfaces and boundaries.

Referring to the 'Thin Film – Plastic Interface' a clear $\sqrt{t}$ response can be seen. This is indicative of pulsed heating of a thin film on the surface of a semi-infinite substrate, giving confidence in the model's physical realism. As the POI are located further from the skin surface there is an expected delay before temperature rise is observed, and when a change is observed, it is of a shallower gradient in both accent and decent.

Numerical Heat Transfer: Plastic Medical Film

To analyse the detrimental effect on accuracy/sensitivity of a plastic medical film, four simulations were performed as detailed in **Table 2**, from which the temperature traces can be directly compared. All other parameters were set to baseline levels with the exception of β, which changed depending on the medium which the thin film is in contact with for each design point.

Table 2: Required simulation design points to evaluate the effects of the plastic medical film.

Design Point (DP) #	Medical Film	Cancerous Test Skin
1 (Baseline)	Y	Y
2	Y	N
3	N	Y
4	N	N

Figure 13 shows the delta temperature trace between the DP1/DP2 pair, the delta temperature trace between the DP3/DP4 pair, and delta between the trace pairs.

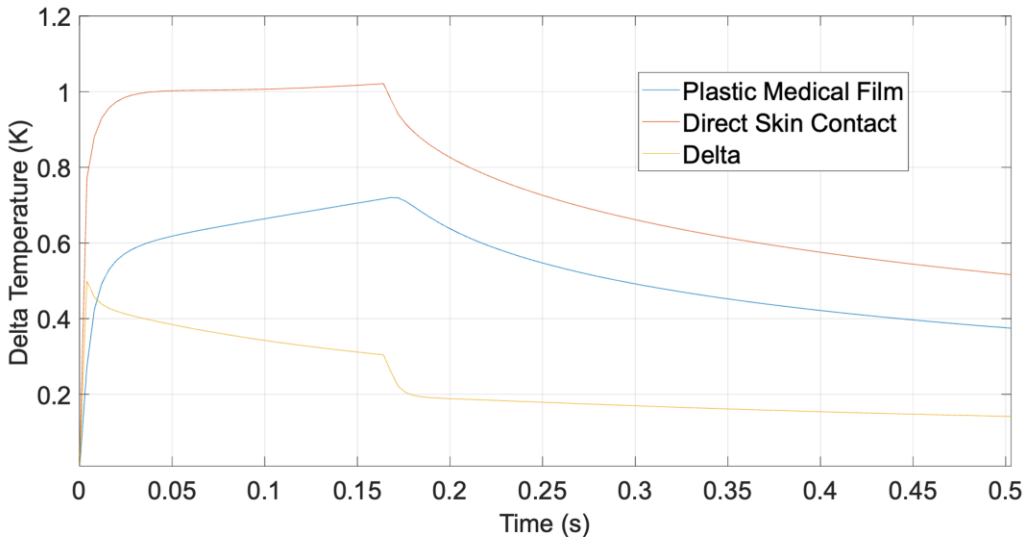

Figure 13: Line plot of the surface temperature against time for the different contact scenario design points.

This analysis clearly demonstrates a maximum sensitivity loss of ~0.5K is incurred as a result of the plastic film at 4 milliseconds. This sensitivity loss decreases with time, or as the temperature gradient differences between each scenario are reduced.

Discussion

The experimental results obtained act as a step towards bringing the sensor to clinical trials. The sensor is shown to operate effectively with a medical film layer for safety, and the heating risk to patients is minimal. However, the experimentation done so far should be considered a preliminary part of a more rigorous testing scheme. The predicted thermal responses are incredibly sensitive to small movements and variations in sensor dimensions, which can be problematic for conducting measurements on patients. Shorting is another potential issue; despite a layer of electrical insulating adhesive covering the sensor's gold contacts, electrical shorting between the platinum filaments and gold contacts may still occur when measuring conductive samples, which will affect the thermal response curve and thus the extracted TP. Further experimentation should be done to determine the impact of these possible issues.

Furthermore, only the thermal response of the ON step was considered in the extraction of the TP so far. The thermal response to the OFF step could also provide valuable data for TP extraction and are expected to contain less electrical noise from the mains. Therefore, TP extraction methods using the OFF step should be explored in a follow-up study.

Conclusions

The Thermal Product Sensor represents a significant advancement in biosensing technology, offering a quantitative, non-invasive method for thermal property measurement. The experimental results validate the sensor's fundamental principles and demonstrate its potential for distinguishing between different biological tissues with remarkable accuracy.

Key contributions of this research include: Simulation and testing of a novel biosensor with precise thermal property measurement capabilities, mathematical modeling of heat transfer dynamics,

experimental validation using porcine tissue samples, investigation of medical film interference in thermal measurements.

Future research directions include refining sensor design, expanding tissue type characterization, and progressing towards clinical trials. The demonstrated sensitivity and precision of the Thermal Product Sensor open new avenues for rapid, non-invasive tissue characterization with potential applications beyond skin cancer diagnosis.

The sensor's ability to provide rapid, quantitative thermal property measurements represents a promising technological approach to addressing the critical need for early and efficient diagnostic techniques in medical research.

References

1. Lawton S. Skin 1: the structure and functions of the skin. Nursing Times [online]; 2019;115:30-33.
2. W Zhang, W Zeng, A Jiang, Z He, X Shen, X Dong, J Feng, H Lu. Global, regional and national incidence, mortality and disability-adjusted life-years of skin cancers and trend analysis from 1990 to 2019: An analysis of the global burden of disease study 2019. Cancer Med. 2021;10(14):4905-4922.
3. Reiter O, Mimouni I, Gdalevich M, Marghoob AA, Levi A, Hodak E, Leshem YA. The diagnostic accuracy of dermoscopy for basal cell carcinoma: A systematic review and meta-analysis. J Am Acad Dermatol. 2019;80(5):1380-1388.
4. Nick et al. “Machine Learning Classification of Skin Lesions Using Thermal Product Biosensing: A Preliminary Diagnostic Approach”. Mega Journal of Case Reports. 2025.
5. D.L Schultz and T.V Jones. Heat-transfer measurements in short-duration hypersonic facilities. University of Oxford, (AGARD), 1973.
6. S.A. Ranamukhaarachchi, S Lehnert, S.L. Ranamukhaarachchi, L Sprenger, T Schneider, I Mansoor, et al. A micromechanical comparison of human and porcine skin before and after preservation by freezing for medical device development. Sci Rep. 2016;6:32074.
7. P Sains, KS Chana, V Sridhar, MS. Sajid. Pilot study on an innovative biosensor with a range of medical and surgical applications. BMC Res Notes. 2018;11(1):81.
8. Pedro Jesús Rodríguez de Rivera, Miriam Lehnert, Rodríguez de Rivera, Fabiola Socorro, Gustavo Marrero Callicó, Jose A. L. et al. Heat flow, heat capacity and thermal resistance of localized surfaces of the human body using a new calorimetric sensor. J Thermal Anal Calorimetry. 2022;147:7385-98.
9. Vaupel P, Piazena H. Strong correlation between specific heat capacity and water content in human tissues suggests preferred heat deposition in malignant tumors upon electromagnetic irradiation. Int J Hyperthermia. 2022;39(1):987-997.
10. Panda S, Das R. A golden section search method for the identification of skin subsurface abnormalities. Inverse Problems Sci Eng. 2017;26(2):83–202.
11. LUNA José Manuel, HERNANDEZ GUERRERO, Abel; ROMERO MENDEZ

Ricardo, LUVIANO ORTIZ José Luis. Solution of the Inverse Bio-Heat Transfer Problem for a Simplified Dermatological Application: Case of Skin Cancer. Ingenier. mecáni. tecnolog. desarroll. 2014;4(6):219-228.

Citation of this Article

Nick N, Kirkup J, Allen M and Chana K. Thermal Product Sensing: Simulations and Experiments of a Novel Biosensor for Quantitative Thermal Property Measurement of Biological Tissues. Mega J Case Rep. 2025;8(6):2001-2019.

Copyright

©2025 Nick N. This is an Open Access Journal Article Published under **Attribution-Share Alike CC BY-SA**: Creative Commons Attribution-Share Alike 4.0 International License. With this license, readers can share, distribute, and download, even commercially, as long as the original source is properly cited.